Published in final edited form as:
J Phys Chem C Nanomater Interfaces. 2011 March 25; 115(15): 7255–7260. doi:10.1021/jp111475y.

Fluorescent Metal Nanoshells: Lifetime-Tunable Molecular Probes in Fluorescent Cell Imaging

Jian Zhang*, **Yi Fu**, and **Joseph R. Lakowicz**
Center for Fluorescence Spectroscopy, University of Maryland School of Medicine, Department of Biochemistry and Molecular Biology, 725 West Lombard Street, Baltimore, MD 21201

Abstract

We reported the preparation of lifetime-tunable fluorescent metal nanoshells and used them as lifetime imaging agents for potential detection of multiple target molecules by a single cell imaging scan. These metal nanoshells were generated to have 40 nm silica cores and 10 nm silver shells. Three kinds of metal-ligand complexes tris(5-amino-1,10-phenanthroline)ruthenium(II) ($Ru(NH_2\text{-}Phen)_3^{2+}$), tris(2,2′-bipyridine) ruthenium(II) ($Ru(bpy)_3^{2+}$), and tris(2,3-bis(2-pyridyl)pyrazine))ruthenium(II) ($Ru(dpp)_3^{2+}$) that have similar excitation and emission wavelengths but different lifetimes were respectively encapsulated in the cores of metal nanoshells for the purpose of fluorescence. Compared with the metal-free silica spheres, these metal nanoshells were found to display enhanced emission intensities and shortened lifetimes due to near-field interactions of Ru(II) complexes with the metal shells. The shortened lifetimes of these metal nanoshells were definitely unique relevant to the Ru(II) complexes: 10 ns for the $Ru(Phen\text{-}NH_2)_3^{2+}$-Ag nanoshells, 45 ns for the $Ru(bpy)_3^{2+}$-Ag nanoshells, and 200 ns for the $Ru(dpp)_3^{2+}$-Ag nanoshells. These lifetimes were longer than the lifetime of cellular autofluorescence (2 – 5 ns), so the emission signals of these metal nanoshells could be distinctly isolated from the cellular background on the lifetime cell images. Moreover, these lifetimes were also different from one another, resulting in the emission signals of three metal nanoshells could be distinguished from one another on the cell images. This feature may offer an opportunity to detect multiple target molecules in a single cell imaging scan when the metal nanoshells are bound with various targets in the cells.

Keywords

fluorescent metal nanoshell; Ru(II) complex; fluorescence cell imaging; molecular imaging agent; near-field interaction; emission intensity; and lifetime

Introduction

Fluorescence cell imaging shows great promise in disease diagnosis or in elucidating cellular signal transduction [1–3]. However, the imaging measurements are often influenced by intrinsic weaknesses of organic fluorophores, including low emission intensity, fast photobleaching, and strong photoblinking [4]. With an advance in fluorescence lifetime imaging microscopy (FLIM), lifetime-resolved fluorescence imaging is now widely used as a valuable tool for cell imaging [5,6]. The use of FLIM may provide certain advantages. First, the lifetime of a fluorophore is typically independent of its concentration. This is

jian@cfs.biomet.umaryland.edu, Tel: 410-706-7500, Fax: 410-706-8409.

Supporting Information Available: TEM images, ensemble absorbance and fluorescence intensity spectra of metal nanoshells. This information is available free of charge via the Internet at http://pubs.acs.org

valuable because the concentrations of local probes are often unknown and changed during the imaging measurements. Second, the concentration change of fluorophores is usually rapid during the image collection due to cellular activities and probe photobleaching. Another advantage of FLIM is that it may provide a way to avoid the cellular autofluorescence which can be observed from almost any cell and tissue. This autofluorescence typically has a lifetime ranging from 2 to 5 ns. On the other hand, most imaging agents are composed of extrinsic organic fluorophores that have similar molecule decay times to the autofluorescence. Thus, the emission signals of probes cannot be distinctly isolable from the present autofluorescence in lifetime cell imaging. The development of novel molecular imaging agents becomes necessary for lifetime cell imaging.

The nanoparticle probes have been developed to use as lifetime imaging agents for cell imaging [7,8]. We are interested in the metal nanoparticles and have worked on this subject in past years [9,10]. It is known that a metal nanoparticle can create a plasmon resonance on its surface, which, in turn, emits light when interacting with a fluorophore in near field [11–14]. As a result, the optical properties of fluorophores may be greatly improved by the near-field interaction, including enhanced emission intensity, increased photobleaching, and reduced photoblinking [15–17]. Importantly, with increased radiative rate of fluorophore that is caused by the interaction of fluorophore with the metal, the lifetime of fluorophores can be dramatically shortened [18]. This feature is now used to design the fluorescence metal nanoparticle probes for cell imaging. We are particularly interested in the metal nanoshells [19,20], because the light-induced interior electric fields in the cores are estimated to be uniform and thus the fluorophores throughout the core can be coupled equally and efficiently for maximal interaction [21].

In our early report, the metal nanoshells have been prepared as imaging agents for detection of genomic targets in cells or target receptors on cell surfaces [22,23]. These metal nanoshells mostly contain the long-lifetime metal-ligand complexes or lanthanides in the cores for fluorescence purpose [19,20,24]. We are likely to detect multiple target molecules in a singe lifetime cell imaging test, which may increase the accuracy and sensitivity in clinical diagnosis [25,26]. In this report, the metal nanoshells with tunable lifetimes were generated in this research and used as molecular imaging agents for lifetime cell imaging. These metal nanoshells were synthesized by encapsulating three kinds of metal-ligand complexes: $Ru(NH_2\text{-}Phen)_3^{2+}$, $Ru(bpy)_3^{2+}$, and $Ru(dpp)_3^{2+}$ respectively in the cores. These three metal-ligand complexes are known to have close excitation and emission wavelengths but different lifetimes [27,28]. The optical properties of as-prepared metal nanoshells were detected on a lifetime-resolved confocal microscope at single nanoprobe level. The metal nanoshells were bound with the avidin molecules and subsequently conjugated with the biotin sites on the cell surfaces. The fluorescence intensity and lifetime cell images were recorded on the confocal microscope, and the results showed that the emission signals of these metal nanoshells could be distinctly separated each other on the lifetime cell images. This observation provides a great potential for detection of multiple target molecules in the cell by a single cell imaging scan.

Materials and Methods

All reagents and spectroscopic grade solvents were used as received from Sigma-Aldrich. Nanopure water (>18.0 MΩ.cm) was purified on Millipore Milli-Q gradient system and used in all experiments. Rhodamine 6G-avidin conjugate was available from Invitrogen. Tris(5-amino-1,10-phenanthroline)ruthenium(II) ($Ru(NH_2\text{-}Phen)_3^{2+}$), tris(2,2′-bipyridine)ruthenium(II) ($Ru(bpy)_3^{2+}$), and tris(2,3-bis(2-pyridyl)pyrazine))ruthenium(II) ($Ru(dpp)_3^{2+}$) complexes were obtained from CFS stock.

Preparation of avidin-bound fluorescent metal nanoshells

The metal nanoshells were made with the silica interior cores and silver external shells in a strategy as described previously [19,20]. The silica spheres were first synthesized in a Stöber method [29]. Typically, three metal-ligand complexes $Ru(Phen\text{-}NH_2)_3^{2+}$, $Ru(bpy)_3^{2+}$, and $Ru(dpp)_3^{2+}$ (5×10^{-6} M) were respectively dissolved with tetraethyl orthosilicate (1.4×10^{-2} M) in alcohol solution. 0.5 mL of 30% ammonium hydroxide was added dropwisely under vigorous stirring. The Ru(II) complex-incorporated silica spheres were observed to form in solution by hydrolysis. These silica spheres were recovered by centrifugation followed by being animated by 3-aminopropyltrimethoxy silane. The metal nanoshells were subsequently deposited on the silica spheres layer-by-layer [19,20]. To improve the chemical stability of metal nanoshells, the metal nanoshells were capped by the organic monolayers of hexa(ethyleneglycol)mono-11-(acetylthio)undecyl ether [30].

The organic monolayers on the metal nanoshells were partially substituted by 11-mercapto-undecanoic acid *via* a ligand exchange reaction to bind with the avidin molecules [31]. Typically, the silver nanoshells (1×10^{-8} M) and 11-mercapto-undecanoic acid (1×10^{-6} M) were co-dissolved in a mixture solvent of ethanol and water (v/v = 1/1). The solution was stirred for 24 h at room temperature. The suspension was removed by centrifugation, and the recovered metal nanoshells were rinsed with ethanol and water, respectively. The metal nanoshells (1×10^{-8} M) were dissolved with the avidin (1×10^{-6} M) in 10 mM phosphate buffered saline (PBS) buffer at pH 8.2 followed by adding excess amount of 1-ethyl-3-(3-dimethylaminopropyl)-carbodiimide hydrochloride (EDC, 2×10^{-5} M) as condensation agent [32]. The solution was stirred at 4°C for 2 h, and the avidin-Ag complexes were recovered by centrifugation and rinsed with 10 mM PBS buffer at pH 7.4. The avidin-Ag complexes were further purified by dialysis against 10 mM PBS buffer at pH 7.4 and then dispersed in 10 mM PBS buffer for incubation with the cell lines.

Culturing and labeling CEM-SS cell lines with metal nanoshells

The CEM-SS cell line was grown in the RPMI-1640 culture medium (Sigma) supplemented with 10% (v/v) heat-inactivated fetal bovine serum (Atlanta Biologicals Inc. GA) and contained 200 units/ml penicillin, 200 units/ml streptomycin (Invitrogene) and recombinant human interleukin (100U/ml) (Roche, Indianapolis, Indiana, USA) for 6 days prior to the conjugation experiments. The number of cells was counted to be ca. 5×10^6 cells/mL.

The CEM-SS cells in 500 μL aliquots were treated in culture solution with 1.0 nM EZ-link sulfo-NHS-biotin for 30 min [33,34]. Washing with 10 mM PBS buffer solution (pH = 7.2), the surface-biotinylated cell lines were suspended in 500 μL 10 mM PBS buffer solution and labeled with 1 nM avidin-Ag complexes for 1 h [35]. All cell samples were washed at least three times with 10 mM PBS-Mg solution followed by re-suspending in 500 μL of 10 mM PBS buffer solution. 20 μL cell-suspended solutions were taken and cast on the cleaned glass coverslips and dried in air for the cell imaging measurements on a lifetime-resolved confocal microscope.

Spectral, imaging, and TEM measurements

Absorption spectra were determined on a Hewlett Packard 8453 spectrophotometer. Ensemble fluorescence spectra were performed on a Cary Eclipse Fluorescence Spectrophotometer. For the transmission electron micrograph (TEM) measurements, the nanoparticle samples were diluted to nano-molar scale, and cast on the copper grids (200 mesh) with standard carbon-coated Formvar films (200–300 Å). The samples were dried in air. The images were taken with a side-entry Philips electron microscope at 120 keV. The size distributions were analyzed with Scion Image Beta Release 2 on the base of at least 100 images.

The fluorescence image measurements were performed on a time-resolved scanning confocal microscope (MicroTime 200, PicoQuant), which consists of an inverted confocal microscope coupled to a high-sensitivity detection setup. A single mode pulsed laser diode (470 nm, 100 ps) was used as the excitation source. An oil immersion objective (Olympus, 100×, 1.3NA) was used for focusing the laser light onto the sample and collecting the emission signal. The emission passed a dichroic mirror, focused onto a 75 μm pinhole for a spatial filtering to reject out-of-focus signal, and finally recorded on a single photon avalanche diode (SPAD) (SPCM-AQR-14, Perkin Elmer Inc). Bandpass filters were used to eliminate the excitation residual. The data collected with a TimeHarp 200 board were stored in the Time-Tagged Time-Resolved Mode (TTTR) that allows every detected photon with its individual timing and detection channel information.

Results and Discussion

The spherical silica nanoparticles were first synthesized as the templates of interior cores of metal nanoshells. Three kinds of metal-ligand complexes $Ru(Phen\text{-}NH_2)_3^{2+}$, $Ru(bpy)_3^{2+}$, and $Ru(dpp)_3^{2+}$ were absorbed in the silica for the fluorescence purpose, which was shown by the color of formed silica spheres although the absorbance spectra could be determined because of their strong light scattering. According to the changes on the complex concentrations in solution before and after reactions, it was estimated that there were *ca*. 5×10^{-4} M $Ru(Phen\text{-}NH_2)_3^{2+}$, 4×10^{-4} M $Ru(bpy)_3^{2+}$, and 3×10^{-4} M $Ru(dpp)_3^{2+}$ complex in the silica spheres. According to the TEM images (Figure S1), the silica spheres were observed to have an average diameter of 40 nm. Per silica sphere thus was estimated to contain approx. 150 $Ru(Phen\text{-}NH_2)_3^{2+}$, 120 $Ru(bpy)_3^{2+}$, or 90 $Ru(dpp)_3^{2+}$ complexes. These Ru(II) complexes were strongly absorbed in the silica spheres and no significant release was observed during store or reaction.

The silica spheres were used as the interior temples for deposition of external metal shell layer-by-layer [19,20]. On the TEM images (Figure S1), the silver shells that were built on three kinds of silica spheres were observed to have similar sizes of 60 nm. The silica spheres are known to have an average diameter of 40 nm. The metal shells thus were estimated to be approx. 10 nm thick. These silver nanoshells also had homogenous size distributions [36]. The absorbance spectra of them showed almost the same plasmon resonances at 430 nm (Figure S2 – S4). Upon excitation at 450 nm, the $Ru(Phen\text{-}NH_2)_3^{2+}$-Ag, $Ru(bpy)_3^{2+}$-Ag, and $Ru(dpp)_3^{2+}$-Ag nanoshells displayed the emission maximums at 596 (Figure S2), 605 (Figure S3), and 608 nm (Figure S4), respectively, close to the emission maximums of free Ru(II) complexes or silica spheres. Similar excitation and emission maximums of three metal nanoshells may promise that the emission signals of them can be detected in a single imaging test when they are bound with multiple target molecules in the cells.

To increase the chemical stability of as-prepared metal nanoshells in buffer solution, they were capped with the monolayers of glycol-like organic ligand [30]. The monolayer-protected metal nanoshells were found to disperse well and stably in 10 mM PBS buffer without significant aggregation for a long time store. The metal nanoshells were partially substituted with the carboxylate-terminal ligands and subsequently bound with the avidin molecules in the presence of excess amount of EDC in solution [31]. To verify the occurrence of binding and determine the binding number, the silica spheres without the Ru(II) complexes were also made and the metal shells were deposited in the same strategy. Under the same conditions, the Rhodamine 6G-avidin conjugates were covalently bound on the metal nanoshells without fluorescence as control [32]. Upon excitation at 510 nm, the control sample of metal nanoshell exhibited an emission maximum at 552, consistent to the Rhodamine 6G-avidin conjugates, indicating that the avidin conjugates were bound on the metal nanoshells. The binding number was determined by a NaCN treatment [37]. Typically,

several drops of 0.1 M NaCN aqueous solution were dropwisely added in solution with the Rhodamine 6G-Ag complexes. The color of plasmon resonance in solution progressively disappeared with time indicating that the metal shells were dissolved by NaCN. The avidin conjugates on the metal shells thus were released into solution. The concentration of metal nanoshell was determined by the intensity of plasmon resonance before metal dissolution, and the concentration of avidin conjugate was determined by the emission intensity after metal dissolution. The binding number on per metal nanoshell thus was estimated by the molar ratio of avidin conjugate over metal nanoshell, which was 6.4 in this case. With the same reaction conditions, the Ru(II) complex-Ag nanoshells were regarded to have approximately similar binding numbers.

The optical properties of single avidin-Ag complexes were recorded on a time-resolved confocal microscope. Prior to casting on the coverslips, the avidin-Ag complexes were diluted to nano mole in solutions. Thus, most metal nanoshells on the coverslips were supposed to be present as individuals. The emission signals recorded on the microscope were thus regarded mostly from the single metal nanoshells. Representative intensity/lifetime emission images were presented in Figure 1, showing that the avidin-Ag complexes were much brighter than the metal free silica spheres. The lifetimes of Ru(II) complexes in the silica was also observed to be shortened by the metal shells. For each sample, at least 50 emission spots were collected for analysis of optical properties, including emission intensity (Figure 2) and lifetime (Figure 3). Compared with the silica spheres, the avidin-Ag complexes showed approx. 6-fold enhancements on the emission intensities almost independent of Ru(II) complexes. On contrary, even though all lifetimes of Ru(II) complexes were dramatically shortened by the metal shells, the scales of decrease were variable depending on the Ru(II) complexes. The lifetime of $Ru(Phen\text{-}NH_2)_3^{2+}$-Ag shells was shortened from 100 ns to 10 ns, a 10-fold decrease; and the lifetime of $Ru(bpy)_3^{2+}$-Ag shells was shortened from 600 ns to 45 ns, a 13-fold decrease. Due to the instrumental limitation, the lifetime of $Ru(dpp)_3^{2+}$in the silica spheres could not be accurately determined. According to literature, the lifetime of $Ru(dpp)_3^{2+}$ in aqueous solution is over 3 μs [22,23]. As immobilized in silica, the lifetime should be increased. Even though the lifetime of 3 μs was used as the $Ru(dpp)_3^{2+}$ in the silica, there was an approx. 17-fold decrease when the lifetime of $Ru(dpp)_3^{2+}$-Ag complexes was determined to be 180 ns. Thus, we can conclude that a longer lifetime complex may result in a greater decrease on the lifetime by the metal shell. This tendency of the lifetime is contrary to that of the intensity. The reason is uncertain. Probably, it can be ascribed to the various processes on the near-field interaction. Enhanced emission intensity is regarded from the coupling interaction of fluorophore with the plasmon resonance of metal nanoparticle on the excitation and emission. Three Ru(II) complexes are known to have close excitation and emission maximums, and the plasmon resonances from three metal nanoshells are also found to have similar maximums. Consequently, three Ru(II) complexes should have similar coupling interactions with the metal shells, resulting in close enhancement efficiencies on the emission intensity. In contrary, a decreased lifetime by the metal nanoshell results in an increase of radiative rate of fluorophore [17,18]. It is a dynamic process and thus is relevant to the lifetime of fluorophore prior to binding with the metal. Consequently, the change on the lifetime for the fluorescence metal nanoshells cannot be completely consistent with that on the emission intensity.

On the other hand, we also notice that the shortened lifetimes of metal nanoshells are still longer than the lifetimes of cellular autofluorescence on the cell images. Thus, we expect the emission signals of them are able to isolate from the cellular background. Importantly, these three Ru(II)-Ag nanoshells exhibit unique and distinctly different lifetimes so their emission signals are expected to be distinguishable on the lifetime cell images. To study the optical properties of metal nanoshells on the cells, CEM-SS cell lines were first surface-biotinylated

by EZ-link sulfo-NHS-biotin [33,34] followed by incubating with three avidin-Ag complexes, respectively, for cell imaging on [35]. The representative cell images were shown in Figure 4. Because we controlled the numbers of biotin-sites on the cell surfaces, only few numbers of nanoprobes were bound on the cells (Figure 4). As expected, only few numbers of emission signals from the metal nanoshells were observed on the collected cell images because of their stronger emission intensities and longer lifetimes in comparison with the cellular autofluorescence. For the emission intensity, the ratio of intensity by the avidin-Ag complexes over average intensity by the cellular background was estimated to be approx. 3. It is this reason that the emission of avidin-Ag complexes could be distinctly isolated from the cellular backgrounds on the intensity cell images. Because of interference from the cellular autofluorescence, the lifetimes of avidin-Ag complexes were significantly shortened in comparison with the lifetimes of them prior to binding with the cells (Figure 3). In fact, the decay curves of avidin-Ag complexes on the cell images could be resolved in double components. The shorter component that was about 3 ns could be ascribed to the cellular autofluorescence and longer component (different values depending on the Ru(II) complexes in the metal nanoshells) was ascribed to the emission from the avidin-Ag complexes.

For each avidin-Ag complex, at least 30 emission spots on the cell images were collected to analyze the apparent lifetimes from the avidin-Ag complexes. The histograms revealed different lifetimes for the three avidin-Ag complexes: 7 ns for the $Ru(Phen\text{-}NH_2)_3^{2+}$-Ag complexes, 17 ns for the $Ru(bpy)_3^{2+}$-Ag complexes, and 42 ns for the $Ru(dpp)_3^{2+}$-Ag complexes (Figure 5). We also noticed that there is no significant overlapping for the histogram curves from the avidin-Ag complexes with the curve from the cellular autofluorescence, indicating that the emission signals from three avidin-Ag complexes could be separated from the cellular backgrounds on the lifetime cell images. In addition, the curves of three Ru(II)-Ag nanoshells also insignificantly overlapped each other representing that the emission signals of three metal nanoshells could be distinguished on the lifetime cell images.

To verify this point, we co-dissolved the $Ru(Phen\text{-}NH_2)_3^{2+}$-Ag, $Ru(bpy)_3^{2+}$-Ag, and $Ru(dpp)_3^{2+}$-Ag complexes at the molar ratio of 1/1/1 in 10 mM PBS buffer followed by incubating with the surface-biotinylated CEM-SS cell lines. By emission intensity and lifetime cell imaging, the emission signals of these metal nanoshells could be detected suggesting that Ru(II)-Ag complexes were bound on the cell surfaces (Figure 6). On the fluorescence intensity cell images (Figure 6a), the emission signals from the metal nanoshells could be distinguished from the cellular autofluorescence because of their bright emission signals. However, we also noticed that the signals from different Ru(II)-Ag complexes were unable to separate because of their close emission strengths. In contrary, on the lifetime cell images (Figure 6b), the emission signals from these avidin-Ag complexes could be distinguishable each other because of different lifetimes of metal nanoshells. The differences on the lifetime can be also resolved from the emission decay curves, on which the three metal nanoshells show distinctly variable lifetimes with the cellular autofluorescence. In this case, three metal nanoshells were simply bound with the biotin sites on the cells. In future, we expect these metal nanoshells will be bound with different probes followed by conjugating with multiple target molecules in the cells. The emission signals of them will be isolated from the cellular autofluorescence and be clearly distinguishable from each other on the lifetime cell images. As a result, more than one type of target molecule in the cell will be detected in a single lifetime cell imaging scan. This approach will be beneficial for increasing the detection sensitivity and accuracy in clinical diagnosis and investigating the distributions of multiple target molecules in cells.

Conclusion

In this study, the lifetime-tunable fluorescent metal nanoshells were synthesized as molecular imaging agents for lifetime cell imaging. Three metal-ligand complexes of $Ru(NH_2\text{-}Phen)_3^{2+}$, $Ru(bpy)_3^{2+}$, or $Ru(dpp)_3^{2+}$ were respectively encapsulated in 40 nm silica spheres followed by depositing 10 nm silver layers as the shells. Three Ru(III)-Ag nanoshells of $Ru(Phen\text{-}NH_2)_3^{2+}$-Ag, $Ru(bpy)_3^{2+}$-Ag, and $Ru(dpp)_3^{2+}$-Ag were observed to display similarly enhanced emission intensities but differently shortened lifetimes. With brighter emission signals and longer lifetimes relative to the cellular autofluorescence, the Ru(II)-Ag nanoshells could be distinctly distinguished from the cellular backgrounds on the cell images. Importantly, owing to unique and distinctly different lifetimes, the emission signals from three metal nanoshells could be clearly separated from each other on the lifetime cell images. *We notice that the lifetimes of Ru(II) complexes are shortened by the metal shells, which is not superior to the lifetime imaging by the Ru(II) complexes. However, it is also known that the Ru(II) complexes have low quantum yields so that their emission signals are low and thus cannot be detected at the single probe level. Our results reveal that when the Ru(II) complex-encapsulated silica spheres are coated with the silver nanoshells, the emission intensities are increased greatly. As a result, the emission signals from the metal nanoshells are observed to become clearer because the interference from the cellular autofluorescence becomes relatively weak. In addition, even though the lifetimes of Ru(II) complexes are shortened by the metal shells, the values are still longer than the lifetime of cellular autofluorescence in cell imaging. Thus, the emission signals from the single nanoprobes can be detected.* This result provides an opportunity to determine multiple kinds of target molecules in the cells when these metal nanoshells are used as molecular imaging agents for lifetime cell imaging. Besides encapsulating the lifetime-tunable fluorophore into the cores, the lifetime of metal nanoshells is anticipated to be tuned by changing the structures of metal nanoshells including core sizes, metal species, and metal shell thicknesses when the same fluorophores are encapsulated in the cores.

Supplementary Material

Refer to Web version on PubMed Central for supplementary material.

Acknowledgments

This research was supported by grants from NIH (EB009509, HG-002655, HG005090, EB006521, and CA134386).

References

1. Weissleder R, Tung CH, Mahmood U, Bogdanov A. Nature Biotechnol. 1999; 17:375. [PubMed: 10207887]
2. Willets KA, Nishimura SY, Schuck PJ, Twieg RJ, Moerner WE. Acc Chem Res. 2005; 38:549. [PubMed: 16028889]
3. (a) Thoumine O, Ewers H, Heine M, Groc L, Frischknecht R, Giannone G, Poujol C, Legros P, Lounis B, Cognet L, Choquet D. Chem Rev. 2008; 108:1565. [PubMed: 18447398] (b) Fang X, Tan W. Acc Chem Res. 2010; 43:48. [PubMed: 19751057]
4. Lakowicz, JR. Principles of Fluorescence Spectroscopy. 3. Springer Published; New York: 2006.
5. Berezin MY, Achilefu S. Chem Rev. 2010; 110:2641. [PubMed: 20356094]
6. Kwak ES, Kang TJ, Bout DAV. Anal Chem. 2001; 73:3257. [PubMed: 11476223]
7. (a) Hayat, MA., editor. Colloidal Gold: Principles, Methods, and Applications. Academic Press; San Diego: 1991. (b) Feldheim, DL.; Foss, CA. Synthesis, Characterization and Applications. Marcel Dekker, Inc; New York: 2002. Metal Nanoparticles.

8. El-Sayed MA. Acc Chem Res. 2004; 37:326. [PubMed: 15147173]
9. Hubert C, Rumyantseva A, Lerondel G, Grand J, Kostcheev S, Billot L, Vial A, Bachelot R, Royer P, Chang S-h, Gray SK, Wiederrecht GP, Schatz GC. Nano Lett. 2005; 5:615. [PubMed: 15826096]
10. Alvarez-Puebla RA, Ross DJ, Nazri GA, Aroca RF. Langmuir. 2005; 21:10504. [PubMed: 16262313]
11. Sokolov K, Chumanov G, Cotton TM. Anal Chem. 1998; 70:3898. [PubMed: 9751028]
12. Kummerlen JLA, Brunner H, Aussenegg FR, Wokaun A. Mol Phys. 1993; 80:1031.
13. Watanabe K, Menzel D, Nilius N, Freund HJ. Chem Rev. 2006; 106:4301. [PubMed: 17031988]
14. (a) Schwartzberg AM, Zhang JZJ. Phys Chem C. 2008; 112:10323.(b) Kamat PVJ. Phys Chem B. 2002; 106:7729.
15. Lakowicz JR. Anal Biochem. 2001; 298:1. [PubMed: 11673890]
16. Lakowicz JR. Anal Biochem. 2005; 337:171. [PubMed: 15691498]
17. Zhang J, Fu Y, Liang D, Nowaczyk K, Zhao RY, Lakowicz JR. Nano Lett. 2008; 8:1179. [PubMed: 18341300]
18. Zhang J, Fu Y, Chowdhury MH, Lakowicz JRJ. Phys Chem C. 2008; 112:18.
19. Stoermer RL, Keating CDJ. Am Chem Soc. 2006; 128:13243.
20. Zhang J, Fu Y, Lakowicz JRJ. Phys Chem C. 2007; 111:1955.
21. Zhang J, Gryczynski I, Gryczynski Z, Lakowicz JR. J Phys Chem B. 2006; 110:8986. [PubMed: 16671705]
22. Lal S, Clare SE, Halas NJ. Acc Chem Res. 2008; 41:1842. [PubMed: 19053240]
23. a) Enderlein. J Phys Chem Chem Phys. 2004; 4:2780.(b) Enderlein J. Appl Phys Letter. 2002; 80:315.
24. Terpetschnig E, Dattelbaum JD, Szmacinski H, Lakowicz JR. Anal Biochem. 1997; 251:241. [PubMed: 9299022]
25. Chatterjee SK, Zetter BR. Future Oncol. 2005; 1:37. [PubMed: 16555974]
26. Varella-Garcia M, Kittelson J, Schulte AP, Vu KO, Wolf HJ, Zeng C, Hirsch FR, Byers T, Kennedy T, Miller YE, Keith RL, Franklin WA. Cancer Detect Prev. 2004; 28:244. [PubMed: 15350627]
27. Goze C, Chambron J-C, Heitz V, Pomeranc D, Salom-Roig XJ, Sauvage J-P, Morales AF, Barigelletti F. Eur J Inorg Chem. 2003:3752.
28. Dobrucki JWJ. Photochem Photobio B: Bio. 2001; 65:136.
29. Stober W, Fink A, Bohn EJ. Colloid Interface Sci. 1968; 26:62.
30. Huang X, Peng X, Wang Y, Wang Y, Shin DM, El-Sayed MA, Nie S. ACS Nano. 2010; 4:5887. [PubMed: 20863096]
31. Templeton AC, Wuelfing WP, Murray RW. Acc Chem Res. 2000; 33:27. [PubMed: 10639073]
32. Brinkley M. Bioconjugate Chem. 1992; 3:2.
33. Wersinger C, Vernier P, Sidhu A. Biochemistry. 2004; 43:1242. [PubMed: 14756560]
34. Wersinger C, Sidhu A. Biochemistry. 2005; 44:13612. [PubMed: 16216085]
35. Zhang J, Fu Y, Liang D, Zhao RY, Lakowicz JR. Anal Chem. 2009; 81:883. [PubMed: 19113832]
36. Zhang J, Fu Y, Mei Y, Jiang F, Lakowicz JR. Anal Chem. 2010; 82:4464. [PubMed: 20433154]
37. Rosi NL, Mirkin CA. Chem Rev. 2005; 105:1547. [PubMed: 15826019]

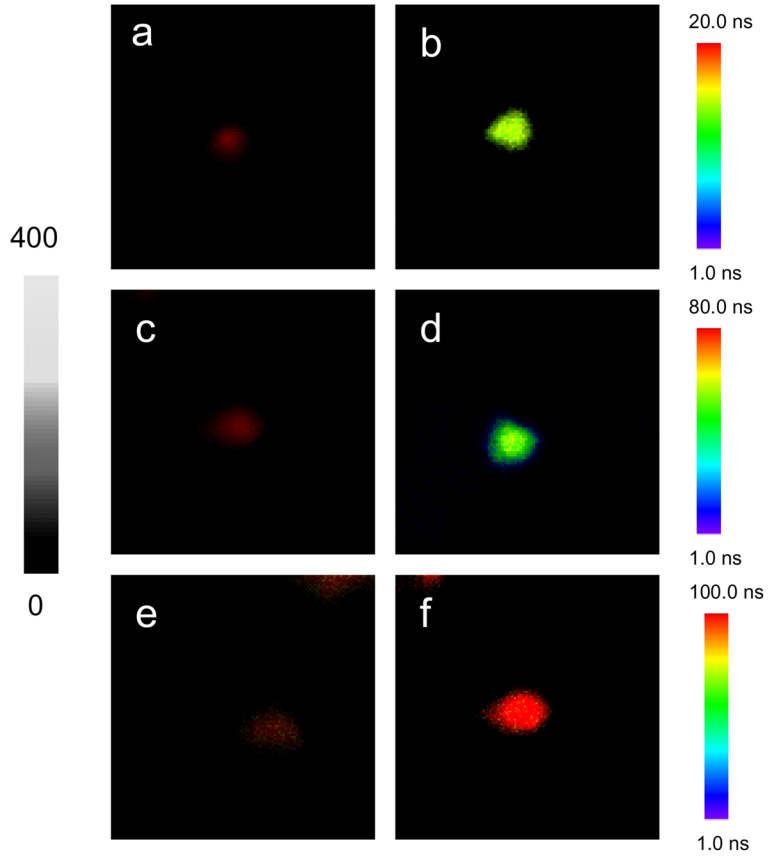

Figure 1.
Typical single nanoshell fluorescence images for (a) $Ru(phen\text{-}NH_2)_3^{2+}$/silica sphere, (b) $Ru(phen\text{-}NH_2)_3^{2+}$-Ag shell, (c) $Ru(bpy)_3^{2+}$/silica sphere, (d) $Ru(bpy)_3^{2+}$-Ag shell, (e) $Ru(dpp)_3^{2+}$/silica sphere, and (f) $Ru(dpp)_3^{2+}$-Ag shell recorded in the emission intensity and lifetime. The scales of diagrams are 5 × 5 μm and the resolutions are 100 × 100 pixel with an integration of 0.6 ms/pixel.

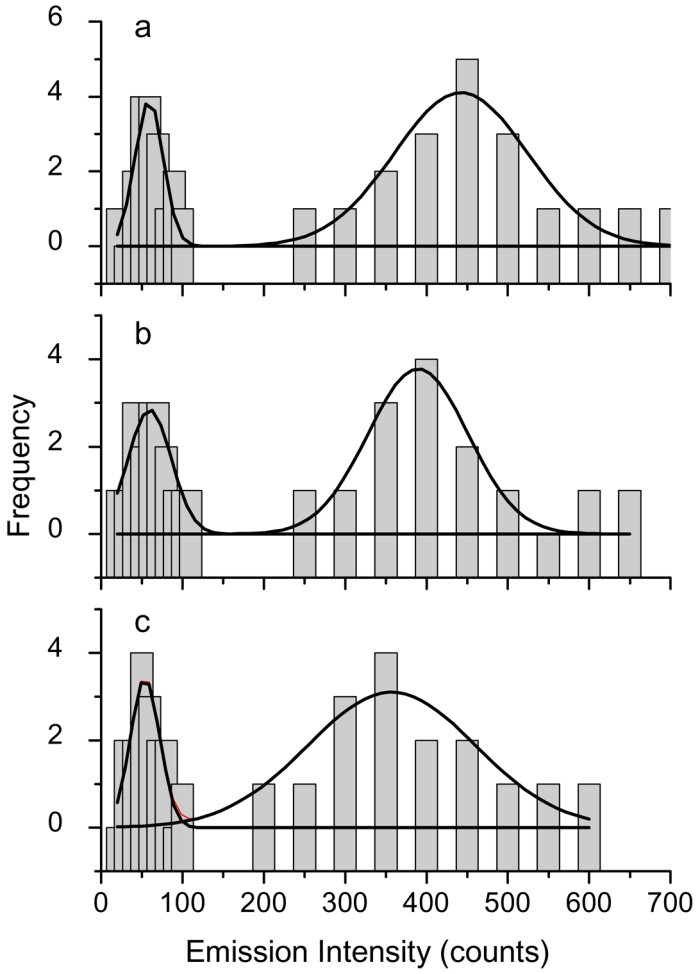

Figure 2.

Histograms of emission intensities from (a) $Ru(phen\text{-}NH_2)_3^{2+}$/silica sphere and $Ru(phen\text{-}NH_2)_3^{2+}$-Ag shell, (b) $Ru(bpy)_3^{2+}$/silica sphere and $Ru(bpy)_3^{2+}$-Ag shell, and (c) $Ru(dpp)_3^{2+}$/silica sphere and $Ru(dpp)_3^{2+}$-Ag shell.

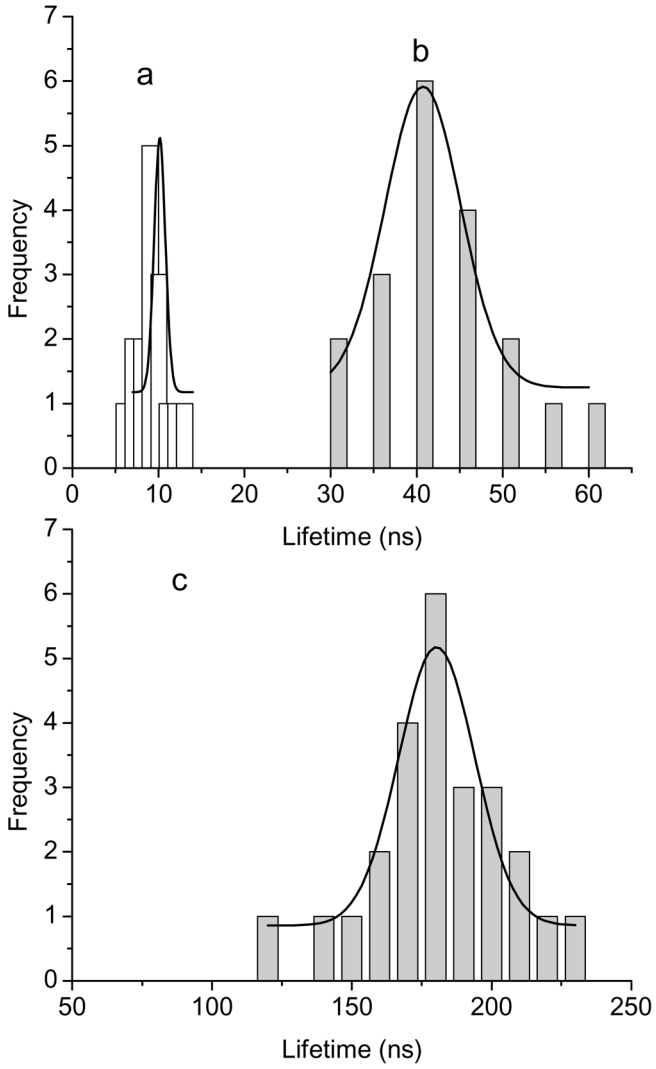

Figure 3.
Histograms of lifetimes from (a) Ru(phen-NH_2)$_3^{2+}$-Ag shells, (b) Ru(bpy)$_3^{2+}$-Ag shells, and (c) Ru(dpp)$_3^{2+}$-Ag shells that were collected from the single nanoprobe images.

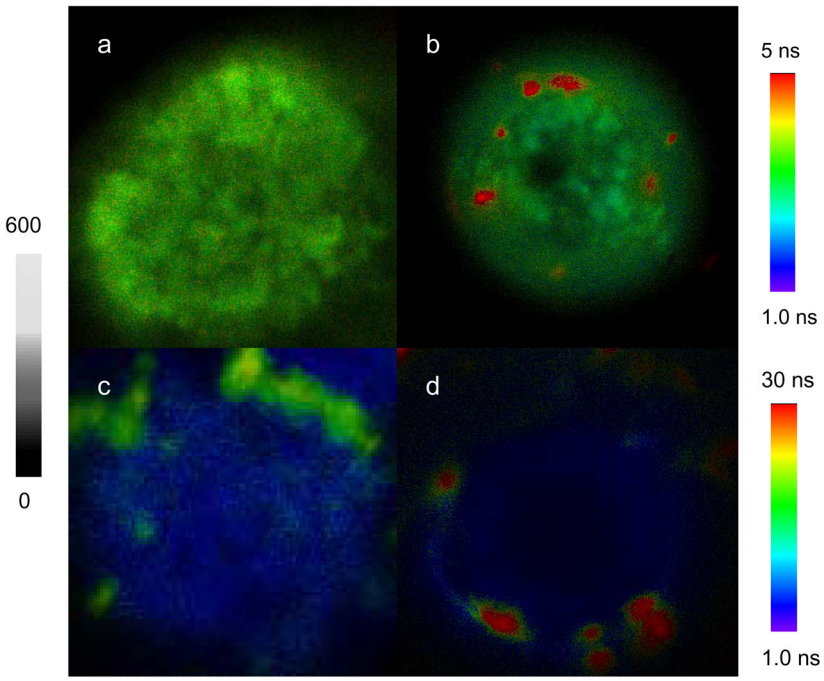

Figure 4.

Representative fluorescence intensity and lifetime images from the single cells (a) blank without dye conjugation, (b) conjugated by $Ru(phen\text{-}NH_2)_3^{2+}$-Ag shells, (c) by $Ru(bpy)_3^{2+}$-Ag shells, and by $Ru(dpp)_3^{2+}$-Ag shells. The scales of diagrams are 15 × 15 μm. The resolutions of diagrams are 100 × 100 pixel with an integration of 0.6 ms/pixel.

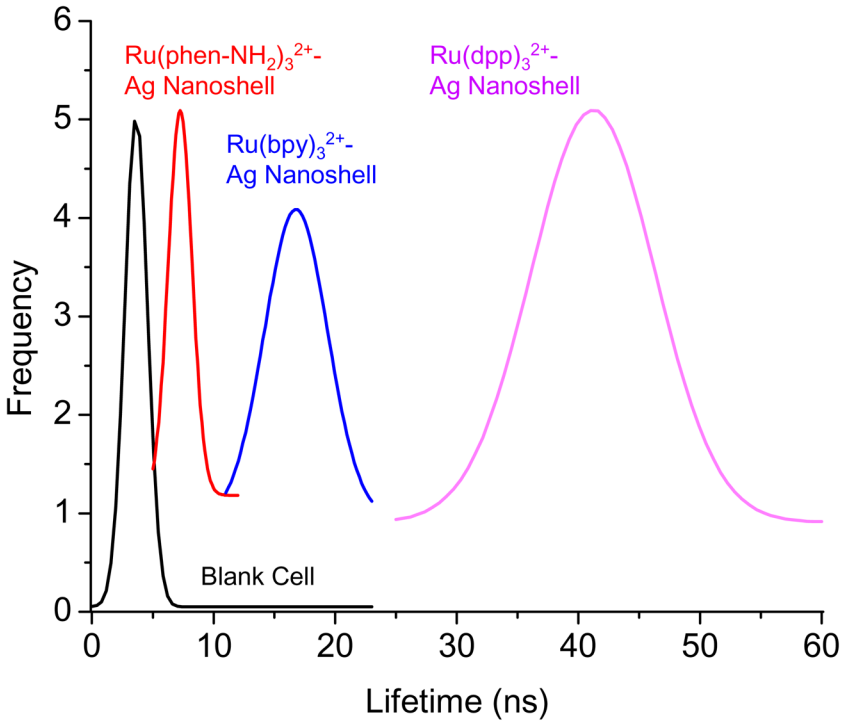

Figure 5.
Histograms of lifetimes from the entire images throughout the blank cells without dye conjugation, and the emission spots from the $Ru(phen\text{-}NH_2)_3^{2+}$-Ag shells, $Ru(bpy)_3^{2+}$-Ag shells, and $Ru(dpp)_3^{2+}$-Ag shells that were conjugated on the cell surfaces.

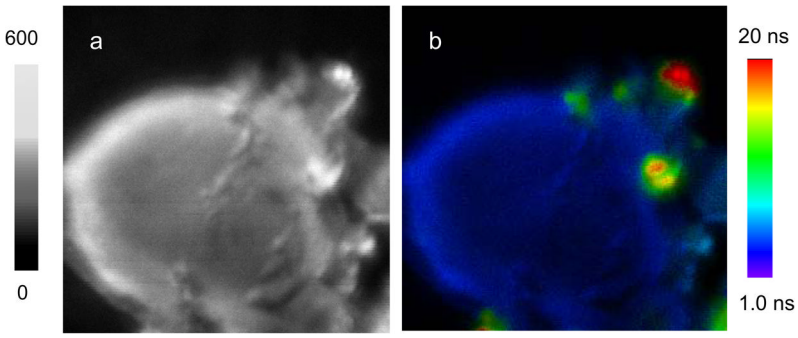

Figure 6.
Representative fluorescence (a) intensity and (b) lifetime cell images conjugated by the $Ru(phen\text{-}NH_2)_3^{2+}$-Ag shells, $Ru(bpy)_3^{2+}$-Ag shells, and $Ru(dpp)_3^{2+}$-Ag shells upon the excitation at 470 nm. The scales of diagrams are 15 × 15 μm. The resolutions of diagrams are 100 × 100 pixel with an integration of 0.6 ms/pixel.